CrossMark

Pull-in-free design of electrically actuated carbon nanotube-based NEMS actuator assuming non-parallel electrodes arrangement

Hassen M. Ouakad[1]

Abstract

In this numerical investigation, the nonlinear structural response of an electrostatic carbon nanotube (CNT) based nano-actuator assuming a non-parallel (out-of-plane) plates actuation configuration is examined. The actuating force is initiated by the asymmetry of the resultant electric fringing-fields caused mainly due to the non-parallel electrodes scheme. The nano-actuator is designed based on a carbon nanotube flexible moving electrode and two symmetrically located actuating stationary rectangular-shaped out-of-plane electrodes. First, the electrical problem of the nano-actuator is numerically solved to acquire the resultant actuating force. The force is then mathematically approximated from the outcomes of a 2D numerical solution of the electric problem via a finite-element-based numerical analysis. Then, the structural behavior of the CNT-based nano-actuator under the effect the resultant non-parallel electric fields is investigated numerically via a modal expansion process. The electro-mechanical model was constructed based on an Euler–Bernoulli continuous non-linear beam model, where both the mid-plane stretching (geometric nonlinearity) and the electric non-parallel fringing-fields effects have been taken into consideration. The reduced-order model (ROM) was derived using the Galerkin decomposition via modal decomposition process. The resultant nonlinear equations are solved numerically to get the static response of the considered CNT-based nano-actuator for various DC voltages. The eigenvalue problem is afterward derived and studied to get the variation of the fundamental as well as higher-order natural frequencies when the system is deflected by a non-zero DC amplitude. A detailed parametric study indicates an opportunity of having larger stroke as well as higher fundamental natural frequency for such CNT-based nano-actuator function of the assumed DC voltage amplitude, enabling it to be used as a tunable NEMS-based device without any pull-in scenario.

Keywords NEMS · Carbon nanotube · Out-of-plane electrodes · Large stroke · Higher tunability · Pull-in free

1 Introduction and background

With the recent developments in the manufacturing technologies of micro- and nano-devices [mainly micro- and nano-electromechanical systems (MEMS and NEMS)], the opportunity for designers in this area still exist for developing novel micro- and nano-systems capable of self-stimulation (sensing and actuating) and with an active and fast response.

## 1.1 Use of parallel-plates electrodes geometry

Deformable electrodes-based capacitors have been tremendously reported and investigated in the literature as great candidates for sensing, actuating, resonating and switching purposes in the nano-scale, for example. To cite one example, the capacitive flexible parallel electrodes have been of great concern as substitutes for conventional semiconductor devices (Fig. 1a). However, theses flexible electrodes showed great sensitivity to an electro-mechanical instability known as the pull-in instability [1, 2] in the micro- and nano-scales. This phenomenon has been first reported in soft materials [3], and then demonstrated with closely spaced thin-films [4]. In fact, when a flexible-electrode based actuator is subjected to a voltage, it bends down to the actuating stationary electrode. Thus, any voltage increase induces an increasing electric field on the

Technical Editor by Pedro Manuel Calas Lopes Pacheco.

✉ Hassen M. Ouakad
   houakad@kfupm.edu.sa

1 Department of Mechanical Engineering, King Fahd University of Petroleum and Minerals, Dhahran 31261, Kingdom of Saudi Arabia

Fig. 1 Parallel-plates electric actuation technique: **a** for $V_{DC} = 0$ Volt, **b** for $V_{DC} < V_{pull-in}$, **c** for $V_{DC} > V_{pull-in}$

(a)   **(b)**   **(c)**
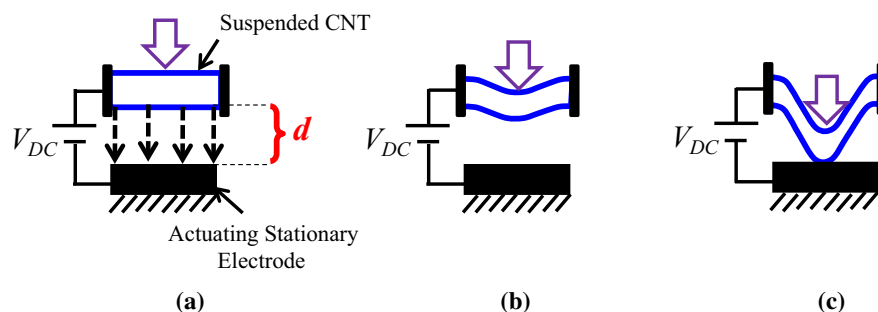
actuator and hence an increasing attractive electric force between the oppositely charged electrodes (Fig. 1b). At a certain voltage threshold (universally called the pull-in voltage), the attractive electric force causes the actuator to move down severely, resulting in a short circuit between the oppositely charged electrodes (Fig. 1c). This is a main electromechanical instability encountered when assuming the parallel-plates capacitive configuration as an actuation technique and is called the pull-in instability (Fig. 1c). Recently, a review article [5] presented a thorough overview on the pull-in structural instability challenges in MEMS and NEMS devices. They pronounced and deliberated on numerous state-of-the-art methodologies for extending the range of travel (stroke) as well as the pull-in instability of electrically actuated NEMS sensors and actuators.

1.2 Pull-in instability control for desired characteristics in MEMS and NEMS devices

Fundamentally, few important applications of electromechanical-based nano-actuators require generation of large displacements rather than large forces. Consequently, keeping electrostatically actuated NEMS devices operating in a stable state, i.e., away from the pull-in instability, presents a major interest for designers in this area and mainly from design, fabrication, and application point of view [5]. Though the electrostatic actuation technique suffers from some limitations such as the pull-in instability, it compromises one of the prevalent energy concentrations existing to-date. Therefore, there is a need for smart design of nano-actuator that simultaneously provide actuation and strain amplification, as well as much larger strain amplification than for ordinary mechanical amplifiers. This challenge has encouraged scientists in recommending new designs and approaches to avoid such structural instabilities (such as the pull-in), and therefore, increase the range of travel of flexible micro- and nano-electrodes.

It is worth mentioning that there is a great necessity for numerous commercial products to design micro- and nano-actuators with some other featured characteristics (other than the extending the range of travel) such as: fast

response, higher efficiency, and with maximum strain. Therefore, numerous control methods have been established to solve the pull-in instability in electrostatic actuators. Many attempts were reported to be successful in extending the range of travel of electrostatically actuated micro- and nano-systems by adding external structures [5]. These suggested external mechanical structures presented excellent success in amplifying the displacements of the electromechanical micro- and nano-devices, however revealed practical limits on the amplification factor, as well as penalties on the overall actuator performance. In addition, few efforts [6–8] have been successful in designing such actuators and are mainly in the micro-scale such as the work done by Rosset et al. [6]. They built a dielectric elastomer (DE) based actuator that showed promising characteristics such as: flexibility in bending (compliant), high-deformation strains (hence large-stroke), and high-conductivity. However, they revealed that these DE-based flexible actuator present a lower compliance capability and, as an alternative, they suggested carbon nanotubes (CNTs) based actuator mainly because of their high and isotropic compliance. Commonly and as formerly explained, electrostatic-attractive-based actuators have a trivial stroke principally because of the electrostatic pull-in instability. Motivated by this, Olfatnia et al. [7] fabricated and tested a MEMS comb-drive actuator with large stroke. Their design was mainly by adopting the conventional comb-drive configuration by adding to it a parallelogram flexure mechanism allowing more compliance and hence further stroke. This amendment in their proposed design allowed not only larger stroke, but also helped in delaying the initiation of the pull-in instability and therefore provide greater actuation stroke. Hu et al. [8] explored the possibility to use an electrostatic-repulsive spring based actuator as a method to achieve large strokes and get rid of any structural instability. Their micro-actuator design shows encouraging use in various applications such as: switches, relays, inductors, and MEMS micro-mirrors.

Despite the enormous successful breakthrough in the fabrication of nano-scale devices, there also still a need in the industry of nano-engineering to satisfy the requirement of precision displacement with a significant stroke. NEMS

devices such as nano-actuators [9–13], nano-switches [14, 15] and nano-resonators [16, 17], etc., are pushed to compete unswervingly with the well-known complementary metal–oxide–semiconductor (CMOS) transistors in performance, the adoption of the single-nanostructure architectures will potentially facilitate the highest levels of performance, although this will also involve overcoming enormous scientific and technological challenges. In this regard, there are plenty of attempts to investigate the feasibility of building tiny systems with large-stroke and possibly having nano-scale resolutions. To cite few, Wang et al. [9] developed 3D Nano driving system with large-stroke and nano-positioning resolution where two actuators were adopted: servomotors to actuate the coarse driving, and piezoelectric actuators to actuate the fine driving. Wei et al. [10] established a suitable grey box model mainly to simulate the deformation of a large stroke gear shaped nano-mirror. Tian at el. [11] demonstrated a novel split-ladder photonic crystal cavity, which can be tuned across a very large wavelength range by an on-chip integrated NEMS actuator. Lambrecht et al. [12] designed and fabricated a shape memory alloy-based NEMS silicon actuator functional as optical ultra-small footprint switching. Again such configuration are good, but not to the top. They are limited in terms of stroke and not much flexible in their bending regime. Keplinget et al. [13] devised smart design for pull-in-free actuators offering an unlimited actuation range and an extra range of deformability. Their design was principally based on an electrode-free configuration of the actuator and where the applied electric field was dictated by the applied voltage due to a nearly constant thickness of the dielectric elastomers coated based actuator and the absence of actuating electrodes.

As it is not possible to construct large-scale arrays of NEMS devices at present, it is also not possible to perform needed experimental characterization to fully optimize the device designs such as the geometries and materials identifications [18]. Therefore, analytical and numerical models that can predict the coupled nonlinear multi-physics response of such nano-devices will become increasingly important [18].

1.3 Carbon nanotube-based nano-structures

The use of discrete particles as useful electronic devices was first proposed back in early 1970s [19]. Formerly, molecular electronics [20, 21] has attracted abundant attention, mostly as it could lead to theoretically new miniaturization approaches in the electronics and computer industry. The apprehension of single-molecule-based devices has persisted to be challenging, mostly due to complications in realizing electrical contact to separable distinct molecules. However, recent developments in the

nanotechnology field have resulted in electrical measurements on single molecules-based structures [22–25]. Among the familiar single molecules-based nano-structures, carbon nanotubes (CNTs) are getting an increasing attention in terms of research to be used as building block for several NEMS devices. Thanks to their distinguished mechanical and electro-thermal properties, CNTs were used in numerous promising applications including super-capacitors, lightweight electromagnetic shields, energy storage and conversion devices; field-emission displays; and nanometer-sized probes [26, 27], semi-conductors [28], mass/force sensors [29, 30], nano-actuators [30–32] or even as nano-materials for artificial muscles [33–36]. Some of these applications are now recognized as outstanding commercial products, whereas others are still under thorough tests and investigations. This is mainly due to the nanotubes cost, and limitations in cost and time-effective processing and assembly methods [26].

Carbon nanotube-based nanostructures are of pronounced importance not only for their basic scientific richness, but also because they have the potential to reform the future commercial application as well as the forthcoming technologies. The use of these miniature devices over the past century has profoundly affected the human communication, computation, manufacturing and transportation systems [37]. Recently, there have been dramatic parallel advances in the miniaturization of electromechanical devices. Commercial MEMS devices now extend the sub-millimeter to micrometer size scale, and there is intense concern in the conception of the next-generation nano-scale electromechanical systems.

1.4 Large-stroke CNT-based NEMS devices

Large-stroke nano-devices are of a colossal practical interest in many applications, but, to-date, few types have been commercially exploited. Typical challenges include slow response, low strain and force generation, short cycle life, use of electrolytes, and low energy efficiency. Consequently, carbon nanotubes were shown to be sole components to build new artificial muscles thanks to their giant elongations and elongation rates, respectively [38]. Furthermore, and in addition to extending the capabilities of artificial muscles to giant strokes and strain rates at extreme temperatures, CNT-based actuator mechanisms provide other possible applications that relate to its light-emitting displaying ability [38], switching capabilities [39, 40], transducing and oscillating capacities [41–43], and large-stroke actuation competencies [44–52].

The application of CNTs for converting electrical energy to mechanical work is suggested by the exceptionally high mechanical properties of the individual nanotubes [53] and the availability of promising actuation

mechanisms, using the accessibility of nanoscale structural features. Several types of actuation processes have been reported for CNT-based NEMS devices, including non-Faradaic actuation by double-layer charge injection [54], electrostatic actuation [55] and light-driven actuation [56]. Several previously actuators were reported to provide large stroke such as strain-biased electrostrictive actuators, low-voltage conducting polymer actuators, electromechanically generated strains actuators, chemically driven micro-gel actuators. However, no electrically driven actuators have been reported that provide large actuator strains and high strain rates at low voltages. To quote few, Spinks et al. [47] reported, for the first time, the possibility to build carbon nanotube-based actuator with large strains, assuming extreme electrochemical potentials and with high voltage stability frame. This represented a new actuation mechanism capable of generating an actuator strain of around 300% in the thickness direction of carbon nanotube actuator. Chen et al. [49] fabricated a bending actuator based on aligned CNT/PDMS composites. They demonstrated an exceptional generation of large bending actuation with large stroke at low driving static electrostatic voltage. They suggested their design as potential replacement of conventional CNT-based actuators mainly in various appropriate fields, such as artificial muscles, nano-robotics, nano-sensors, nano-transducers, nano-manipulation, nano-devices for medical applications. Park et al. [50] demonstrated the first case of a macroscopic graphene-based actuator as an alternative to the conventional CNTs based nano-actuators. Though they revealed that the design mechanism of actuation is not yet understood, they consider that this graphene-based actuator is interesting and promising in numerous applications such as gas sensors. Kang et al. [51] demonstrated using molecular-dynamics simulations a carbon nanotube-based gigahertz actuator. Li et al. [52] reported on a single-walled CNT-based electromechanical actuator of remarkable features such as ease of fabrication, lightweight, flexibility, long durability, biocompatibility, low driving actuating voltages, and controllability in air. They consider their design of great prospective for several applications, such as artificial muscles for biomimetic flying insects or robots and flexible deployable reflectors and so on.

1.5 Literature review summary

We can clearly comprehend from the previously and succinctly summarized literature review that electro-mechanical carbon nanotube-based NEMS devices were shown to generate higher stresses than natural muscle and higher strains than high-modulus ferroelectrics [57]. Unlike conventional ferroelectric-based actuators which generate low currents at high voltages, CNT-based nano-actuators could be used to convert mechanical energy to electrical energy for mechanical sensor and energy-conversion devices, and hence would provide high currents at low voltages. This effect is desirable for remotely located sensors, such as seismic-based sensors principally located down-hole in oil exploration applications. Hence, if CNT actuators can be further exploited to provide large mechanical energy (larger displacement), then the output electrical energy per cycle would be much higher than that produced by alternative technologies. This feature, may eventually enable such applications as the conversion of the mechanical energy to electrical energy and hence for energy harvesting purposes.

1.6 Research work objectives and possible contributions

The principal goal of the proposed research investigation is to establish an electro-mechanical model and utilize it to investigate the nonlinear electro-mechanical behavior of CNT-based nano-actuators under a reliable and efficient actuation technique. The reliability and performance of carbon nanotubes-based nano-devices under electric load should be more creative in order to exploit their unique features and extend their use to new applications and products in the nano-scale.

As enlightened before in the introductory part, a critical issue for the commercialization of nano-devices, made with carbon nanotubes as principal components, is their survivability when actuated electrically by the classical parallel-plates type of actuation (Fig. 1). This type of actuation configuration can lead to various damage mechanisms, such as stiction, Fig. 1c, and related short circuit problems (due mainly to the so-called pull-in instability) of the carbon nanotube-based nano-structures. The proposed work aims to suggest a novel and efficient actuation approach that is capable of stimulating the motion of the carbon nanotubes structures without any short circuits problems. One of the configurations we will consider in this particular research is the out-of-plane electric fringing-fields actuation arrangement (Fig. 2). In this arrangement, the resultant actuating load is produced by the unevenness of the fringing-electric fields, mainly due to an out-of-plane asymmetry of the actuated beam (the carbon nanotube in our case) and the two stationary electrodes symmetrically located at its both sides, as shown in Fig. 2. We believe that such research attempt can shed light on the potential of utilizing carbon nanotubes as reliable nano-scale devices and actuators of pull-in-free behavior and with possible large-stroke trend. We plan to demonstrate that this simple configuration can be advantageous for numerous practical electrostatic actuators using carbon nanotubes as basic structures to build in many NEMS devices.

Fig. 2 Fringing-fields electrostatic actuation method. In this figure, the dashed arrows represent the generated electric fields lines for each configuration and the big arrows show the direction of the resultant electrostatic force due to these electric fringing-fields
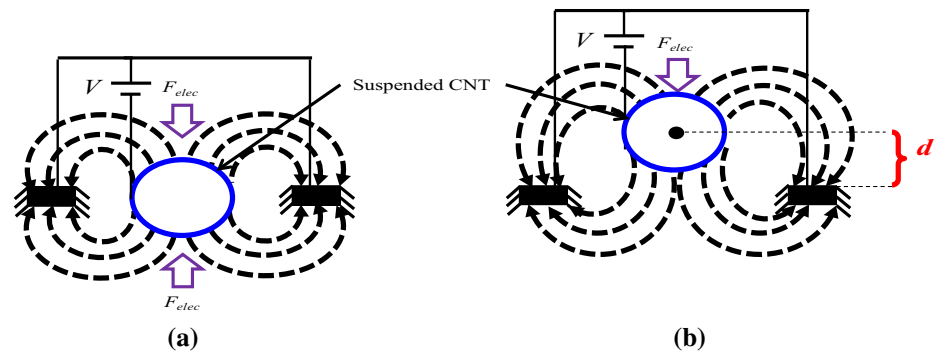
Contributions of this work are the following: first, a finite-element model is implemented to numerically calculate the resultant electrostatic actuating force of the CNT-based nano-actuator as function of the assumed design parameters. Second, analytical expressions for the non-parallel actuating force as function of the electrodes vertical offset distance expressions are examined. Third, an electro-structural nonlinear model is developed and then numerically solved for the static response and the natural frequencies of the CNT-based nano-actuator as function of the DC load. Simulations results demonstrating the influence of the proposed actuator geometrical properties on its resultant electric force as well as its nonlinear structural behavior are discussed.

To this end, the paper is organized as follows: modeling information about the electrical and the electro-mechanical problems of the CNT-based non-parallel plates electrostatic actuator is first discussed in Sect. 2. Then, the evaluation of the resultant electrostatic force using a numerical method is presented in the third section. A parametric study is then carried out to examine the effect of the actuator geometrical properties on its structural behavior in Sect. 4. Finally, Sect. 5 summarizes and concludes on the main results of this investigation.

2 Electro-mechanical model description

2.1 Assessment of the actuating electric force

A simple model governing the electrical behavior of a fringing-fields electrostatic CNT-based nano-actuator as was previously described in Fig. 2 is first formulated. A single flexible CNT-based electrode and two rectangular-shaped stationary electrodes, as shown in Fig. 3a, both supposed to be deposited on the substrate are adopted. It is assumed here that all electrodes are made of a perfectly conductive material. Considering the two-dimensional problem where the electric resultant force will be calculated per unit length, we denote by w_e and t_e the width and the thickness of the symmetric the two stationary

electrodes and by R the radius of the flexible electrode (the CNT). Both actuating electrodes are assumed to be grounded and symmetrically located at both sides of the carbon nanotube with separation offset distance symbolized by d in the vertical z-direction (Fig. 3b). The horizontal separation distance between the actuating non-parallel stationary electrodes and the CNT edges in the (x, y)-plane is represented by the distance g (Fig. 3b). An attractive force symbolized by $F_{electric}$ will be initiated at the surface area of the CNT and having only a non-trivial subsequent component in the z-direction. This attractive force characterizes the electrostatic force per unit length function arising due to asymmetry of the electric fringing-fields between the CNT and both of its stationary side electrodes. Note that this particular function cannot be calculated analytically in a closed form, and will be numerically determined afterward.

A finite-elements method (FEM) is executed to numerically compute this resultant attractive electrostatic force per unit length, i.e., $F_{electric}$ of the fringing-fields electrostatic actuator described in Fig. 3 (see below for more details). This electrical force acting on the moving electrode is a function of the actuator geometrical properties (w_e, t_e, R, g, d) and the air permittivity $\varepsilon_0 = 8.8542 \times 10^{-12}$ F/m. Figure 4a illustrates the 2D finite-elements method schematic model of the electrostatic problem of the CNT-based nano-actuator described in Fig. 3 for a prescribed vertical offset d. The electrostatic field distribution as well as the electrostatic force acting on the movable electrode of Fig. 4a, is solution of a Laplace equation obtained from the following Maxwell–Laplace equations of electro-magnetism:

$$\frac{\partial^2 \varphi}{\partial x^2} + \frac{\partial^2 \varphi}{\partial y^2} + \frac{\partial^2 \varphi}{\partial z^2} = -\frac{\rho}{\varepsilon_0}, \tag{1}$$

where the function "φ" in Eq. (1) symbolizes here the electric potential between the two stationary rectangular electrodes and the movable electrode (the CNT), and ρ represents electric charge density. As for the boundary conditions for the electrostatic potential used to solve the above Maxwell–Laplace equation, Eq. (1), the following
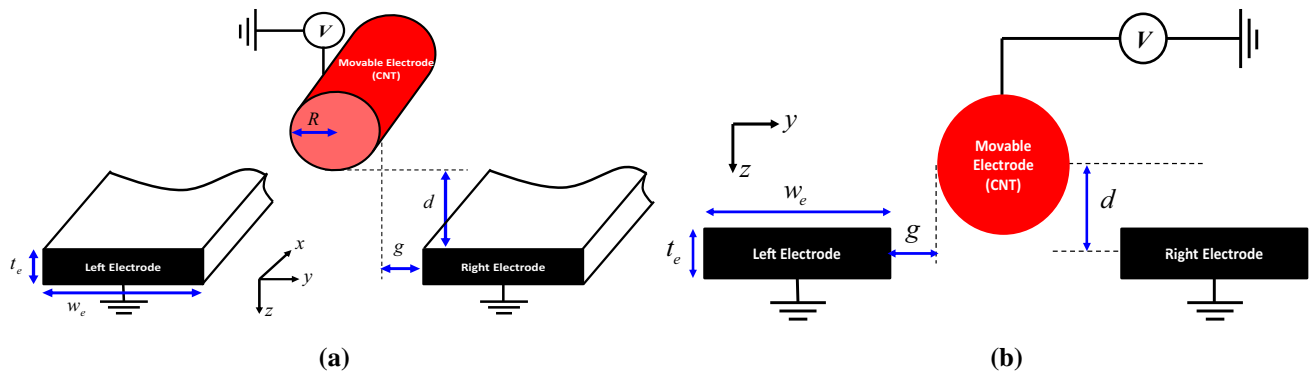
Fig. 3 **a** 3D schematic of the fringing-fields electrostatic actuator, **b** 2D (out-of-plane) view of the actuator
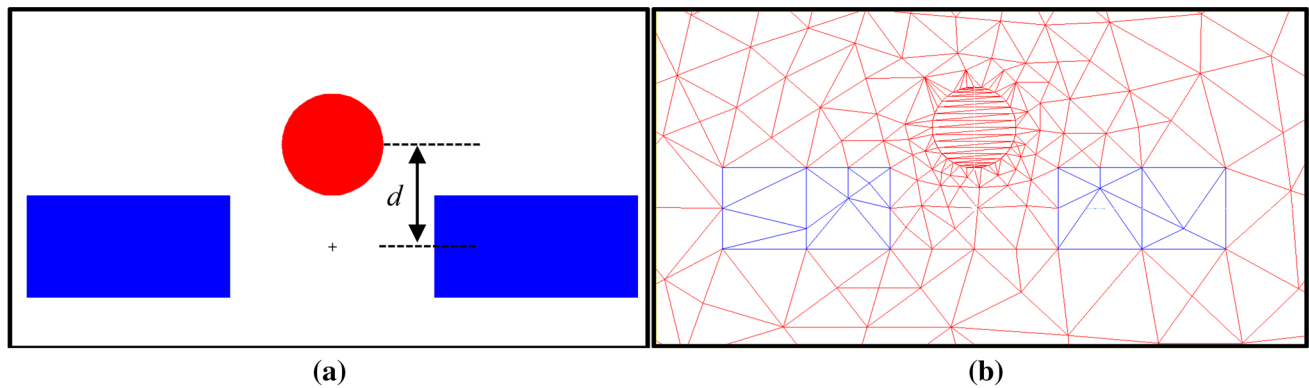

Fig. 4 Planar (2D) finite-element model of the electric problem of the CNT-based nano-actuator shown in Fig. 3

mixed boundary conditions set is considered: a non-homogenous potential $\varphi = 1$ in the neighborhood of the movable electrode (the CNT), and a homogenous condition $\varphi = 0$ is assumed far from the nano-actuator, i.e., for $(x, y, z) \rightarrow \infty$.

As for the adopted general procedure of the finite-element method, our program was built based on the following key steps:

- We first generate a mesh over the domain. The assumed mesh was mainly triangles in order to discretize the domain. We generated the mesh through a software packages available in the Mathworks/Matlab PDE toolbox (Fig. 4b). Each mesh element has three respective nodes, and each node was expressed in terms of the Hermite interpolation functions [58, 59].
- We then construct the finite-element method basis functions (assuming linear Lagrangian interpolation functions) over the generated mesh.
- Next, we assemble the stiffness matrix and the force vector element by element.
- Finally, we solve the system of equations assuming the Newton–Raphson method and then we perform the error calculation: an error of 10^{-4} % was used as a

decision criterion for the convergence and therefore end of each FEM simulation.

As a case study, a perfectly conductive CNT of radius $R = 1$ nm, and a horizontal offset to the actuating rectangular electrodes of $g = 1$ nm. A DC voltage of $V = 1$ V is applied between the CNT and its neighborhood actuating electrodes having both 4 nm width and 2 nm thickness, respectively, is assumed. Furthermore and unless stated, the same geometrical properties of the two actuating electrodes (width and thickness) were both assumed of same values as the movable electrode (i.e., $w_e = 4R$, and $t_e = 2R$). Figure 5a, b displays, respectively, the equipotential lines as well as the electric field when a DC voltage of 1 V is applied across the two stationary electrodes and the CNT for the case of $d = 2$ nm. Here, we assumed that the lengths of both the CNT and its surrounding stationary actuating electrodes to be much larger than their radius and widths, respectively, in order to reduce the influence of the fringing-fields in the neighborhood of the electrodes' boundaries (ends).

Similar process as displayed in Fig. 5a, b can be recurred for different values of the vertical offset parameter d associated with the position of the movable electrode in the vertical z-direction. Therefore, the electrostatic force
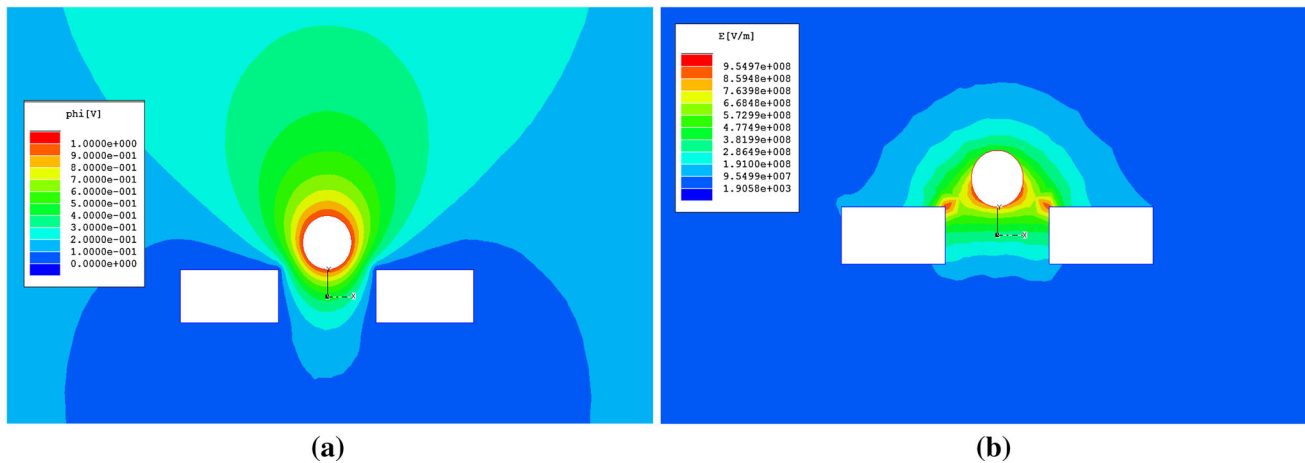
Fig. 5 **a** Equipotential lines, and **b** electric field distribution around the CNT actuator and its surrounding stationary electrodes for $d = 2$ nm

per unit length acting on the flexible electrode (the carbon nanotube) can be calculated as a function of this parameter d, as exposed in Fig. 6. This actuating force acting on the CNT was calculated for multiple prescribed offset distances d. We can clearly apprehend, from Fig. 6, that the numerically calculated electric force per unit length is a nonlinear function of the offset parameter d. First, for small values of d, it rapidly increases making a spike near $d = 2$ nm which is equal to the assumed geometrical parameter g in this case study. Far from this spike, the force slowly decreases toward zero for high values of the offset parameter d.

Next, the obtained numerical electric actuating force per unit length will be fitted by appropriate functions that estimate this force as a function of the offset parameter d.
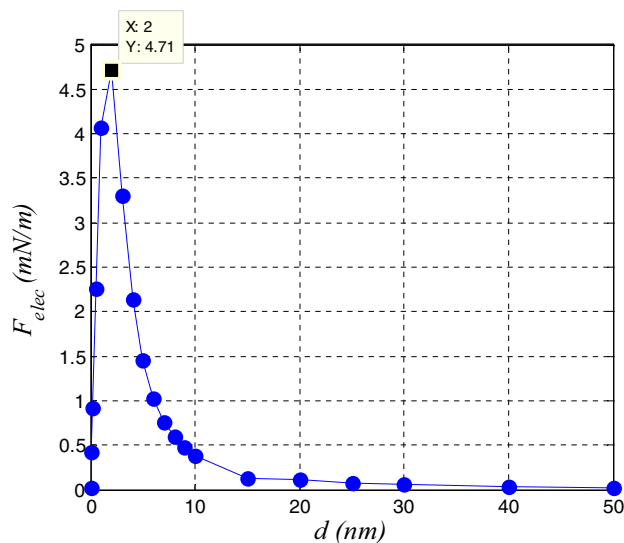

Fig. 6 The subsequent electric force per unit length acting in the z-direction on the flexible CNT electrode as function of the offset parameter d

Though, numerous appropriate fitting mathematical functions can be used in this regard, i.e. [60], in this particular investigation we adopt the following suitable functions:

$$\hat{F}_{electric}(d) = \frac{c_1 d^{c_2}}{1 + c_3 d^{c_4}}. \tag{2}$$

A numerical fitting process was performed for a range of values for the varying the offset parameter d from 0 to 50 nm to get the appropriate fitting factors c_1, c_2, c_3, and c_4. The calculated fitting constants c_1, c_2, c_3, and c_4 of the two different study cases shown in Fig. 7, are summarized in Table 1, respectively.

We can clearly see that the fitting function is in agreement with the numerical electrostatic solution for the range of $0 \leq d \leq 50$ nm and that are somehow reproducing well the electrostatic force generated by the numerical finite-elements electrical model.

2.2 Electro-mechanical model

As carbon nanotubes structural topology are likely to be comparable to beams for small radii, we propose next to adopt a classical continuum Euler–Bernoulli based beam model to simulate the nonlinear structural behavior of the CNT-based nano-actuator (Fig. 8a).

Therefore, the CNT-based flexible electrode is assumed to be made of homogeneous isotropic carbon-based elastic material with mass density $\rho = 1.3$ g/cm^3, Young's modulus $E = 1.2$ TPa. It is modeled as a hollow cylinder of radius R, shell thickness $h = 0.34$ nm, and length L (Fig. 8b, c). Its cross-sectional area as well as its area moment of inertia are denoted by A and I, respectively. In addition, as the surrounding electrodes are symmetrically located at both sides of the flexible CNT electrode with an offset d in the vertical z-direction, Fig. 8c, a distributed electrostatic force will be acting in the surface superficial
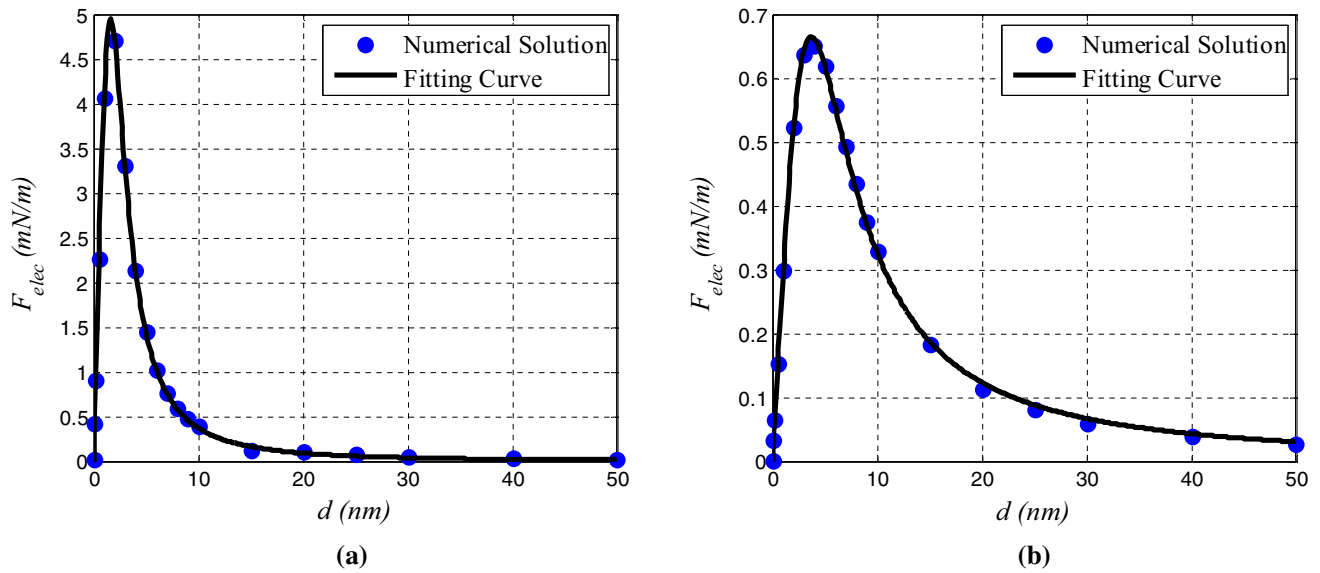
Fig. 7 The electric force obtained by the finite_element model as compared to the fitting function assuming several case studies and for $w_e = 4$ nm, and $t_e = 2$ nm. **a** Case # 01: $g = 1$ nm, $R = 1$ nm. **b** Case # 02: $g = 4$ nm, $R = 1$ nm

Table 1 The appropriate fitting constants for the study cases of Fig. 7

Case study #	c_1	c_2	c_3	c_4
01	4.539×10^{-3}	1.00,313	0.112443	3.03601
02	2.95256×10^{-4}	1.00021	0.0231232	2.54179

area of the nanotube and having only a resultant component in the vertical z-direction, as was exposed previously in the electrical model of Sect. 2.1. We also assume a lateral gap size between both actuating electrodes and the nanotube edge denoted by the parameter g, as shown in Fig. 8b.

As pronounced earlier in this section, the nanotube is assumed to obey the Euler–Bernoulli nonlinear beam the-
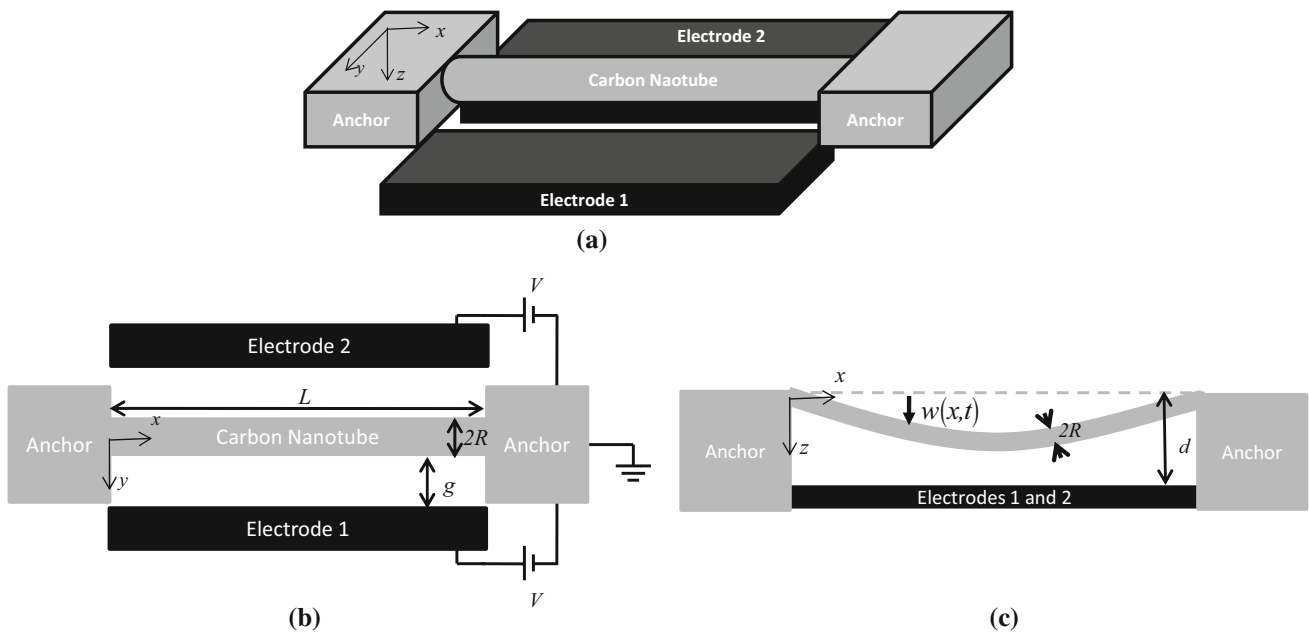

Fig. 8 **a** 3D chart of a carbon nanotube-based nano-actuator under the effect of the fringing electrostatic fields. **b** Top and **c** side view of the nano-actuator

ory as we are supposing that its radius is $R \ll L$ and that its deflection in the z-direction $w(x, t) \ll L$. In addition, we disregard in this problem any rotary inertia and axial (normal) effects compared with the transverse inertia effect which appears here to be the most dominant. Under these assumptions, the equation describing the in-plane displacement $w(x, t)$ of the CNT-based nano-actuator can be written as [61]:

$$EI \frac{\partial^4 w}{\partial x^4} + \rho A \frac{\partial^2 w}{\partial t^2} + c \frac{\partial w}{\partial t} = \frac{EA}{2L} \left(\int_0^L \left(\frac{\partial w}{\partial x} \right)^2 dx \right) \frac{\partial^2 w}{\partial x^2} + V_{DC}^2 F_{electric}(w + d), \quad (3)$$

where c is the viscous damping coefficient and the function $F_{electric}$ symbolizes the distributed resulting electric force per unit length. This particular function can be numerically obtained using a closed form, as was appropriately explained in the electrical model of Sect. 2.1.

The boundary conditions of the actuator are

$$\hat{w}(x = 0, t) = 0, \frac{\partial w}{\partial x}(x = 0, t) = 0, \hat{w}(x = L, t) = 0, \frac{\partial w}{\partial \hat{x}}(x = L, t) = 0. \quad (4)$$

3 Numerical macromodel

3.1 Galerkin-based modal expansion

Any numerical computation can provide abundant and relatively efficient results for complex devices such as MEMS/NEMS. It can also proficiently carry out multi-physics and multi-scales problem simulations. Nevertheless, when one considers tiny complicated structure or even the number of the discrete units to be large, the computing time can be expensive and the numerical resolution tends to be inefficient. Macromodel-based numerical techniques that have been widely used in many areas is a very effective tool to design MEMS and NEMS devices. The most distinguishing property of macromodels is their high efficacy while maintaining a certain solution accuracy. Macromodeling methods have been successfully applied in the design and development of a great many MEMS and NEMS devices. To quote few types of macromodels, we can cite the following [62]: those based on the so-called Galerkin method, macromodels based on trajectory piecewise-linear approach, those based on proper orthogonal decomposition, macromodels based on Krylov subspace projection, macromodels based on neural-network, and analytical macromodels, etc.

In this research work, we propose to use the macromodel based on the Galerkin decomposition. The Galerkin method is an effective weighted residual method for solving the approximate numerical solution of differential equations. The main idea is to represent the unknown field functions using approximation function constituted by the linear combination of a known family of linearly independent basis functions and undetermined parameters. To this end, to get an approximate numerical solution for the unknown in-plane deflection field $w(x, t)$ of the equation governing the CNT-based non-actuator along with its associated limit conditions, Eqs. (3)–(4), these equations are discretized using the Galerkin expansion technique to yield a macromodel. Hence, the in-plane stroke of the CNT-based nano-actuator is estimated as

$$w(x,t) = \sum_{i=1}^{n} \psi_i(x) \mu_i(t), \quad (5)$$

where $\psi_{i=1\ldots n}(x)$ are the presumed basis functions assumed here to be the linear undamped mode shapes of a fixed–fixed CNT nano-beam. The functions $\mu_{i=1\ldots n}(t)$ are denoting time-varying generalized coordinates functions. To acquire the numerical macromodel, we substitute Eq. (5) into Eqs. (3)–(4), multiply for $1 \le j \le n$ by the basis functions $\psi_{j=1\ldots n}(x)$, then use the orthogonality conditions of the basis functions to finally integrate the resultant equations from 0 to L. The outcome would be the reduced-order numerical model in the form of a set of ordinary differential equations (ODEs) all function of the generalized coordinates functions $\mu_{i=1\ldots n}(t)$. These ordinary differential equations can be seen as macromodel representation of the CNT-based nano-actuator.

It is worth to mention here that, in the process of getting the ODEs, the basis functions $\psi_{j=1\ldots n}(x)$ will stay rooted inside the denominator of the electric force assumed function, Eq. (2). A convenient way to resolve this problematic numerical issue and hence live with this complicated resulting integral terms due to that nonlinear electrostatic force, is to consecutively evaluate the spatial integrals containing the spatial functions $\psi_{j=1\ldots n}(x)$ numerically while integrating the ordinary differential equations with respect to generalized coordinates functions $\psi_{j=1\ldots n}(t)$.

3.2 Static and linearized eigenvalue problem solutions

Bearing in mind here to resolve the nonlinear structural behavior of the CNT-based nano-actuator under the out-of-plane electric DC static load, we compute its stationary deflection by setting all time-dependent terms in the ODEs equal to zero. Then the modal amplitudes $\psi_{j=1\ldots n}(t)$ are replaced by unknown constant quantities $k_{j=1\ldots n}$. This results in a system of nonlinear algebraic equations in

terms of those coefficients. The system is then solved numerically using the Newton–Raphson method. We finally plan to investigate the variation of the CNT-based nano-system natural frequencies under the effect of the applied DC out-of-plane voltage by solving the system-linearized eigenvalue problem. To this end, we consider the constructed macromodel discretized equations, which can be re-written in the state-space form as:

$$\dot{\Gamma} = M(\Gamma), \tag{6}$$

where

$$\Gamma = [\mu_1, \mu_2, \ldots, \mu_n]^T, \tag{7}$$

is the actuator generalized coordinates functions vector and M is a right-hand side vector representing the stiffness coefficients and also called the coefficient matrix. The determinant of this coefficient matrix gives the natural frequencies of the inclined riser and the associated mode shapes are obtained from the eigenvectors. Detailed methodology solution of the nonlinear eigenvalue problem can be found in the following references [63–66].

4 Electro-mechanical behavior

The aim of this sub-section is to carry out a parametric study using the electro-mechanical model developed in Sect. 2.2. Subsequently, we propose to run series of numerical simulations in order to examine the influence of the apparent geometrical properties of the actuator (CNT radius, electrodes thickness and width, as well as the lateral gap offset distance g) on its nonlinear structural behavior (static deflections and eigenvalues). We consider in this section, and unless stated otherwise, the same geometrical parameters used to generate the results of Fig. 6, i.e., $R = 1$ nm, $g = 1$ nm, $w_e = 4R$, and $t_e = 2R$. We also assume a hollow cylindrical shape single-walled CNT of mass density $\rho = 1.3$ g/cm^3, Young's modulus $E = 1.2$ TPa, shell thickness $h = 0.34$ nm, and length $L = 1000$ nm.

4.1 Macromodel convergence analysis

The convergence of the numerical outcomes of the constructed macromodel, summarized in Sect. 3.1, can be investigated by comparing the maximum static deflection of the CNT-based nano-actuator while varying the number of assumed basis functions in the Galerkin decomposition, i.e., Equation (4). To this end, Fig. 9 shows the nano-actuator mid-point displacement while assuming one up to seven (symmetric as well as anti-symmetric) mode shapes of a straight clamped–clamped beam as basis functions in

the Galerkin decomposition, while varying the applied DC voltage, and for a vertical offset $d = 10$ nm. It follows from the plot that using five modes yields acceptable converged ($\approx$ accurate) results. Consequently, in the rest of the paper, we will use five mode shapes of a straight beam as basis functions in the Galerkin decomposition.

It can also be understood from the same figure that the CNT static deflection increases steadily for small DC load and then increases suddenly when the electric force reaches its peak point, as explained before in the electric model, to finally converge to the actuator assumed initial vertical offset where the actuating electric force become nearly null. In fact, the CNT max deflection saturates at 10 nm for high DC amplitude as the nano-structure almost reached the vertical position of the actuating electrode and therefore the electric force and the elastic CNT restoring force are both under an equilibrium state. The same figure demonstrates also three different regimes based on the strength of the applied DC load and also function of the location of the CNT mid-point. The first regime is when the beam deflection is in the range where the electric force is increasing steadily (for $d \approx$ 4–10 nm) and hence the CNT mid-point deflection is showing a nonlinear steady increase from 0 to 6 nm. A second regime is experienced by the CNT static profile when the electric force reaches its maximum peak value ($d \approx$ 2–4 nm) and therefore the CNT maximum displacement is displaying a harsh increase from 6 to 8 nm, to finally converge rapidly to the assumed initial value of the vertical offset and this would represent the third regime (for $d \approx$ 0–2 nm, i.e., $w_{max} \approx$ 8–10 nm). Further, it is noted that this mechanical behavior is a bit different from what was formerly reported for electrostatically actuated microbeam of rectangular cross section [61]. This difference is mainly due to the nonlinear flexibility of the carbon nanotube owning cylindrical cross-sectional shape.

4.2 In-plane versus out-of-plane actuation

It is assumed that it might be of countless importance to numerous CNT-based NEMS engineers to comprehend the difference between their respective behavior while triggered by out-of-plane arrangement (like considered in this research paper) to the one when assuming the classical in-plane parallel-plates electrostatic fields. This comparison is demonstrated in Fig. 10. The corresponding figure proves clearly that assuming the nano-actuator while triggering it using an out-of-plane electrostatic force increased its stroke travel range compared to the in-plane (parallel-plates) pattern, therefore, offering the opportunity of a large stroke actuator without any short circuit (pull-in instability) problem as encountered in the in-plane actuation arrangement.
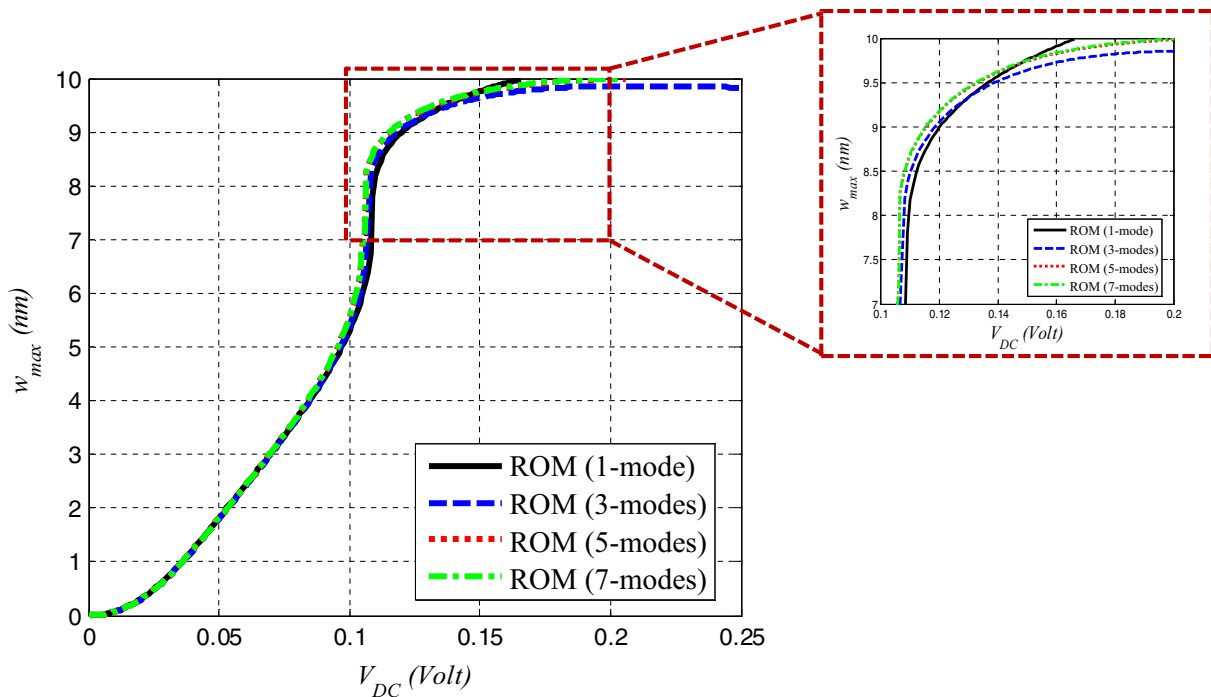
Fig. 9 Variation of the actuator stationary mid-point deflection with the applied out-of-plane DC load for various number of basis functions in the Galerkin-based macromodel and for an assumed vertical offset of $d = 10$ nm
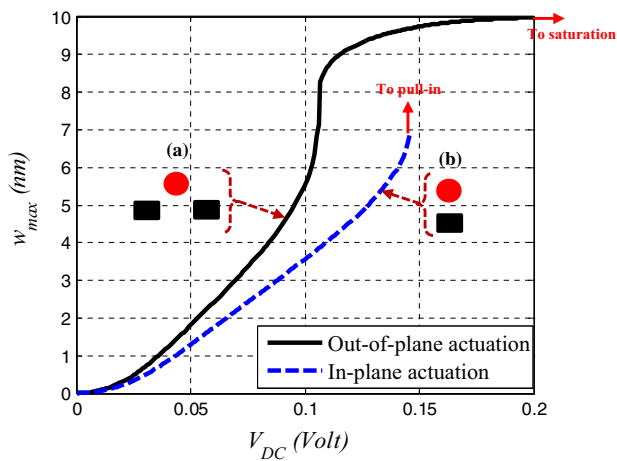

Fig. 10 Evaluation of the difference between the CNT-based nano-actuator static deflection when triggered using **a** out-of-plane actuation arrangement, and **b** in-plane actuation pattern

To compliment what was said before, Fig. 11 reveals that the suggested out-of-plane actuation arrangement for CNT-based nano-actuator could be an excellent candidate of a tunable NEMS device used as wide-bands frequency nano-resonators or even nano-filters as compared to the classical nano-resonators assuming in-plane (parallel-plates) electrostatic actuation design. It can be clearly understood from Fig. 11b, that assuming the in-plane actuation, the tuning fundamental frequency is limited by the pull-in structural instability, where it goes to zero;

whereas, if one considers the second suggested out-of-plane arrangement, one can clearly see that the fundamental frequency, as well as the higher frequencies, are all tunable, Fig. 11a, and their tunability (increase or decrease) is not limited by any structural instability. Moreover, the same figure shows that the higher natural frequencies for the case of out-of-plane actuation are all increasing with the increase the DC voltage as compared to those of the same nano-beam when assuming an in-plane configuration which its higher natural frequencies have been found to be nearly insensitive to the same DC voltage increase (Fig. 11b). Finally, looking carefully at Fig. 11a, one can clearly depict a crossing between the first symmetric and second antisymmetric modes and hence suggesting a possibility of a one-to-one internal resonance between these two respective modes.

4.3 Parametric analysis

In this sub-section, we propose to study further the static and eigenvalue problem bifurcation analysis and complete the complete picture through a comprehensive parametric study. Accordingly, the effect of the CNT radius R, its lateral gap size, and its vertical offset, are investigated, respectively, in Figs. 12, 13 and 14. As seen in the all the quoted figures, the electrically actuated out-of-plane CNT-based nano-actuator maximum mid-point static deflection increases when increasing the DC load, offering the larger
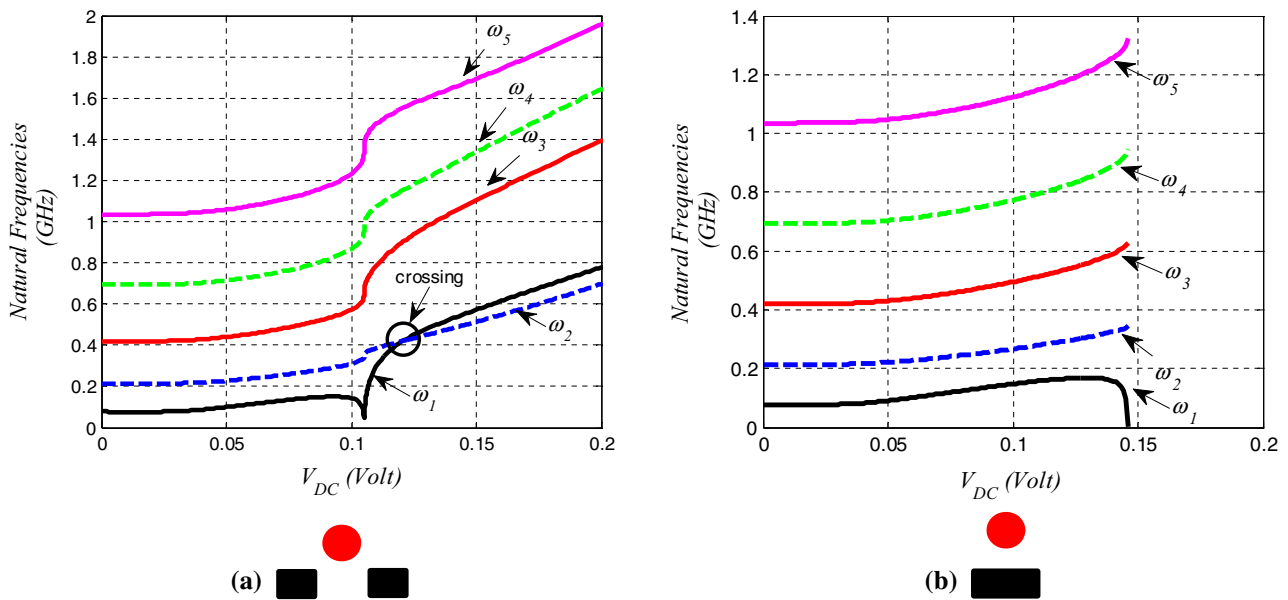
Fig. 11 Comparison between the variation of the first five natural frequencies. The CNT-based nano-actuator with the applied DC load when considering **a** out-of-plane actuation, and **b** in-plane actuation
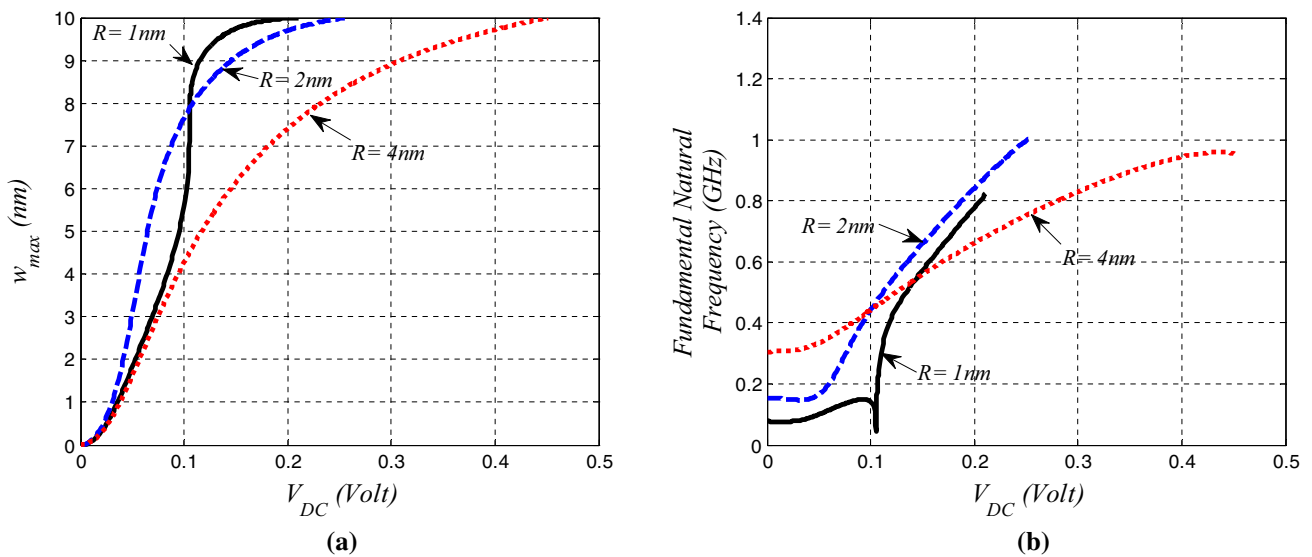

Fig. 12 Variation of the carbon nanotube-based nano-actuator: **a** mid-point deflection, and **b** fundamental natural frequency with the out-of-plane dc voltage amplitude and for various CNT radii

strokes with no-possibility of pull-in structural instability. Similarly, we can see that the fundamental frequency in all considered cases increases monotonically when increasing the out-of-plane DC amplitudes. This is happening because of the cubic geometric nonlinearity of the clamped–clamped CNT, which is of hardening effect, dominating all the way the electrostatic softening nonlinearity, which effect is decreasing with the CNT deflection increase. Furthermore, all figures show that both static maximum deflection as well as its fundamental natural frequency is sensitive to the variation the nano-actuator basic design

parameter as will be exposed with details in the coming sub-sections.

- Effect of the CNT radius

We examine here the effect of the CNT radius "R" on both its static maximum deflection as well as the variation of its fundamental natural frequency with the out-of-plane electric force DC amplitude (Fig. 12). We can realize from the figure that as the CNT radius is further increased, one needs more DC load to further displace it. Also, we can evidently realize from Fig. 12a that there is no strong
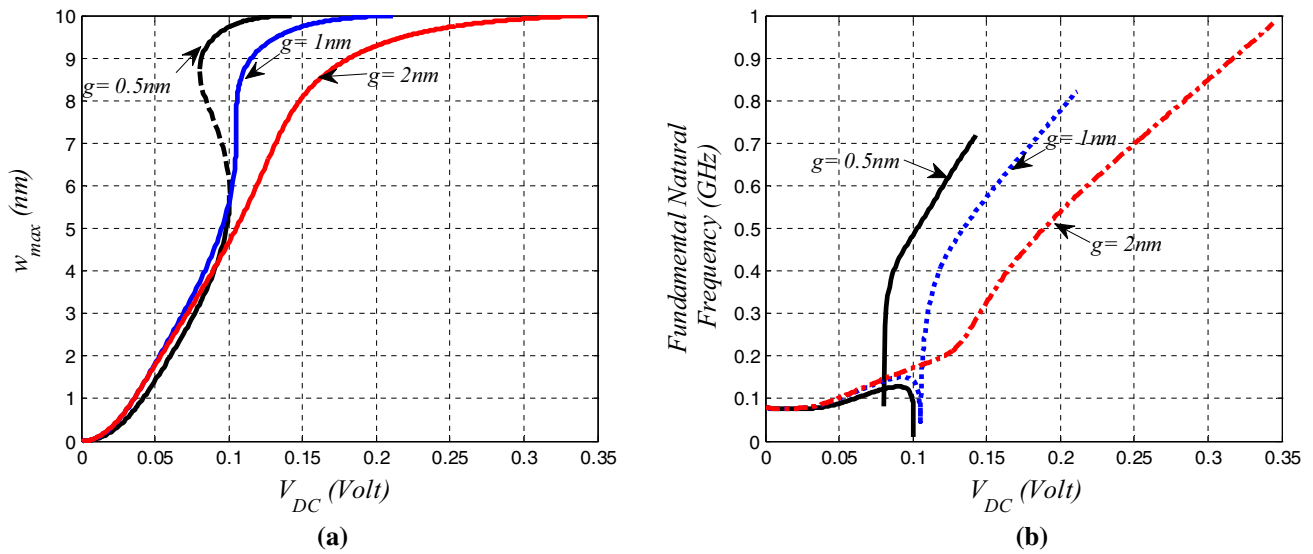
Fig. 13 Variation of the carbon nanotube-based nano-actuator: **a** mid-point deflection, and **b** fundamental natural frequency with the out-of-plane dc voltage amplitude and for various lateral gap sizes
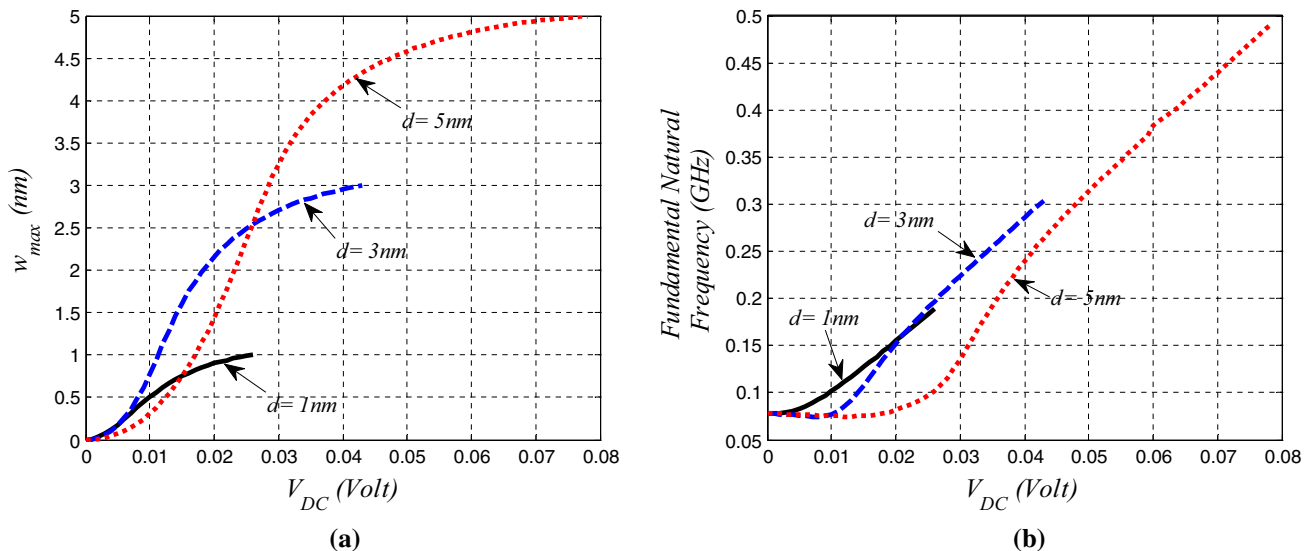

Fig. 14 Variation of the carbon nanotube-based nano-actuator: **a** mid-point deflection, and **b** fundamental natural frequency with the out-of-plane DC voltage amplitude and for various vertical gap sizes

conclusion on which radius is better for large stroke actuator. In fact, for DC load varying between 0 and 0.1 V, Fig. 12a shows that $R = 2$ nm is experiencing larger strokes. Nevertheless, for higher values of DC voltage ($V_{DC} > 0.1$ V), $R = 1$ nm becomes more prominent to be used as larger stroke actuator. This is also displayed in the frequency domain (Fig. 12b). In addition, for lower DC amplitudes, $R = 4$ nm is having the largest fundamental natural frequency. However, for higher DC load values, i.e., $V_{DC} > 0.1$ V, the CNT possessing a radius of 2 nm owns higher values of the fundamental natural frequency offering the possibility to be used as higher-frequency

NEMS-based resonator assuming this particular actuation level.

• Effect of the nano-actuator lateral gap size

The effect of the CNT-based nano-actuator lateral gap size "g" on its static and fundamental natural frequency variation with the applied out-of-plane DC load is investigated and displayed in Fig. 13. An interesting phenomenon arises here. Actually, it can be realized from that for low values of the lateral gap size parameter, the CNT static bifurcation diagram, Fig. 13a, changed from a single-valued to a multi-valued hysteresis band based static behavior. We can also understand from the same figure that

this geometrical design parameter has trivial effect on the CNT maximum stroke for lower values of DC voltages, but then for higher values ($V_{DC} > 0.1$ Volt), lower values of g is showing larger strokes, Fig. 13a, as well as higher natural fundamental frequency values (Fig. 13b).

- Effect of the nano-actuator vertical gap offset

Finally, the effect of the CNT vertical gap size "d" on its static and linearized eigenvalue problem is examined and the outcomes are presented in Fig. 14. Here, and as expected, the more one designs the CNT assuming higher vertical gap size "d", the further the nano-actuator will experience higher stroke range of travel (Fig. 14a). Accordingly, for higher assumed values of this vertical offset size, the nano-actuator will be deflected further and therefore will experience higher fundamental frequencies with the DC load, Fig. 14b, which is principally due to its mid-plane stretching nonlinear hardening effect.

5 Conclusion

In this numerical investigation, the nonlinear electro-mechanical behavior of a carbon nanotube-based nano-actuator when actuated by out-of-plane electric force was exposed and examined. The electric problem was solved numerically by finite-element method to acquire a simple mathematical analytical expression for the resultant nonlinear electric force. Afterward, a static as well as an eigenvalue problem of the out-of-plane nano-actuator has been explored numerically for various values of applied DC voltage amplitudes. A Galerkin modal expansion-based macromodel to get the discretized equations of motion governing the structural behavior of the actuator was constructed. Potential scenarios of large stroke actuator offering the possibility of a simple NEMS device with larger range of travel stroke and without being limited by any structural instability (such as short circuit in parallel plates NEMS-based capacitors) were revealed. Results also showed opportunity to have higher natural frequencies for such nano-actuator offering them chances to be used as wide-band tunable NEMS devices.

In the future, we plan to extend this study by developing a metamodel for the approximation of the electric force for the non-parallel plates CNT-based nano-actuator, which will take into account all its design parameters. An extension of the static study through solving the full dynamical behavior of such CNT-based NEMS devices is also planned.

Compliance with Ethical Standards

References

1. Plante JS, Dubowsky S (2006) Large-scale failure modes of dielectric elastomer actuators. Int J Solids Struct 43:7727–7751
2. Keplinger C, Kaltenbrunner M, Arnold N, Bauer S (2008) Capacitive extensometry for transient strain analysis of dielectric elastomer actuators. Appl Phys Lett 92:192903
3. Stark KH, Garton CG (1955) Electric strength of irradiated polythene. Nature 176:1225–1226
4. Taylor G (1968) The coalescence of closely spaced drops when they are at different electric potentials. Proc R Soc Lond A 306:423–434
5. Zhang W-M, Yan H, Peng Z-K, Meng G (2014) Electrostatic pull-in instability in MEMS/NEMS: a review. Sens Actuators A 214:187–218
6. Rosset S, Shea HR (2013) Flexible and stretchable electrodes for dielectric elastomer actuators. Appl Phys A 110(2):281–307
7. Olfatnia M, Sood S, Gorman JJ, Awtar S (2013) Large stroke electrostatic comb-drive actuators enabled by a novel flexure mechanism. J Microelectromech Syst 22(2):483–494
8. Hu F, Wang W, Yao J (2011) An electrostatic MEMS spring actuator with large stroke and out-of-plane actuation. J Micromech Microeng 21(11):115029
9. Wang S, Du Z, Xie T (2011) A 3D nano driving system with large-stroke. In: Seventh International Symposium on Precision Engineering Measurements and Instrumentation. International Society for Optics and Photonics, pp 832112–832112
10. Wei H-C, John Su G-D (2011) A large-stroke deformable mirror by gear shaped IPMC design. In: 2011 IEEE International Conference on Nano/Micro Engineered and Molecular Systems (NEMS). IEEE, pp 113–116
11. Tian F, Zhou G, Chau FS, Deng J, Akkipeddi R, Tang X, Teo SL, Loke YC (2013) A tunable split-ladder photonic crystal cavity by nanoelectromechanical actuator. In: SPIE MOEMS-MEMS. International Society for Optics and Photonics, pp. 86160Q–86160Q
12. Lambrecht F, Aseguinolaza I, Chernenko V, Kohl M (2016) Integrated SMA-based NEMS actuator for optical switching. In: 2016 IEEE 29th International Conference on Micro Electro Mechanical Systems (MEMS). IEEE, pp 79–82
13. Keplinger C, Kaltenbrunner M, Arnold N, Bauer S (2010) Röntgen's electrode-free elastomer actuators without electromechanical pull-in instability. Proc Natl Acad Sci 107(10):4505–4510
14. Ma JB, Jiang L, Asokanthan SF (2010) Influence of surface effects on the pull-in instability of NEMS electrostatic switches. Nanotechnology 21(50):505708
15. Acquaviva D, Arun A, Esconjauregui S, Bouvet D, Robertson J, Smajda R, Magrez A, Forro L, Ionescu AM (2010) Capacitive nanoelectromechanical switch based on suspended carbon nanotube array. Appl Phys Lett 97(23):233508
16. Piazza G (2010) Aluminium nitride piezoelectric NEMS resonators and switches. In: SPIE Defense, Security, and Sensing.

International Society for Optics and Photonics, pp 76791L–76791L

17. Uranga A, Verd J, Marigó E, Giner J, Muñóz-Gamarra JL, Barniol N (2013) Exploitation of non-linearities in CMOS-NEMS electrostatic resonators for mechanical memories. Sens Actuators A 197:88–95

18. Loh OY, Espinosa HD (2012) Nanoelectromechanical contact switches. Nat Nanotechnol 7(5):283–295

19. Aviram A, Ratner MA (1974) Molecular rectifiers. Chem Phys Lett 29:277–283

20. Carter FL, Siatkowski RE, Wohltjen H (1988) Molecular Electronics Devices. North Holland, Amsterdam

21. Aviram A (ed.) (1992) Molecular electronics—science and technology. In: AIP Conference Proceedings, vol 262

22. Joachim C, Gimzewski JK, Schittler RR, Chavy C (1995) Electronic transparence of a single C60 molecule. Phys Rev Lett 74:2102–2105

23. Tans SJ et al (1997) Individual single-wall carbon nanotubes as quantum wires. Nature 386:474–477

24. Porath D, Millo O (1997) Single electron tunneling and level spectroscopy of isolated C60 molecules. J Appl Phys 81:2241–2244

25. Reed MA, Zhou C, Muller CJ, Burgin TP, Tour JM (1997) Conductance of a molecular junction. Science 278:252–254

26. De Volder MFL, Tawfick SH, Baughman RH, John Hart A (2013) Carbon nanotubes: present and future commercial applications. Science 339(6119):535–539

27. Baughman RH, Zakhidov AA, de Heer WA (2002) Carbon nanotubes–the route toward applications. Science 297(5582):787–792

28. Tans SJ, Verschueren ARM, Dekker C (1998) Room-temperature transistor based on a single carbon nanotube. Nature 393(6680):49–52

29. Mehdipour I, Erfani-Moghadam A, Mehdipour C (2013) Application of an electrostatically actuated cantilevered carbon nanotube with an attached mass as a bio-mass sensor. Curr Appl Phys 13(7):1463–1469

30. Li C, Thostenson ET, Chou T-W (2008) Sensors and actuators based on carbon nanotubes and their composites: a review. Compos Sci Technol 68(6):1227–1249

31. Kim YH, Jun Kim W (2008) Carbon nanotube actuator. U.S. Patent Application 12/196,159, filed August 21, 2008

32. Fennimore AM, Yuzvinsky TD, Han W-Q, Fuhrer MS, Cumings J, Zettl A (2003) Rotational actuators based on carbon nanotubes. Nature 424(6947):408–410

33. Spinks GM, Mottaghitalab V, Samani MB, Whitten PG, Wallace GG (2006) Carbon nanotube reinforced polyaniline fibers for high strength artificial muscles. Adv Mater 18(5):637–640

34. Foroughi J, Spinks GM, Wallace GG, Jiyoung O, Kozlov ME, Fang S, Mirfakhrai T et al (2011) Torsional carbon nanotube artificial muscles. Science 334(6055):494–497

35. Lima MD, Li N, De Andrade MJ, Fang S, Oh J, Spinks GM, Kozlov ME et al (2012) Electrically, chemically, and photonically powered torsional and tensile actuation of hybrid carbon nanotube yarn muscles. Science 338(6109):928–932

36. Vohrer U, Kolaric I, Haque MH, Roth S, Detlaff-Weglikowska U (2004) Carbon nanotube sheets for the use as artificial muscles. Carbon 42(5):1159–1164

37. De Volder MFL, Tawfick SH, Baughman RH, John Hart A (2013) Carbon nanotubes: present and future commercial applications. Science 339(6119):535–539

38. Aliev AE, Oh J, Kozlov ME, Kuznetsov AA, Fang S, Fonseca AF, Ovalle R et al (2009) Giant-stroke, superelastic carbon nanotube aerogel muscles. Science 323(5921):1575–1578

39. Rasekh M, Khadem SE, Tatari M (2010) Nonlinear behaviour of electrostatically actuated carbon nanotube-based devices. J Phys D Appl Phys 43(31):315301

40. Dequesnes M, Rotkin SV, Aluru NR (2002) Calculation of pull-in voltages for carbon-nanotube-based nanoelectromechanical switches. Nanotechnology 13(1):120

41. Weldon JA, Aleman B, Sussman A, Gannett W, Zettl AK (2010) Sustained mechanical self-oscillations in carbon nanotubes. Nano Letters 10(5):1728–1733

42. Sazonova V, Yaish Y, Üstünel H, Roundy D, Arias TA, McEuen PL (2004) A tunable carbon nanotube electromechanical oscillator. Nature 431(7006):284–287

43. Choi W, Hong J (2012) Rapid electromechanical transduction on a single-walled carbon nanotube film: sensing fast mechanical loading via detection of electrical signal change. Ind Eng Chem Res 51(45):14714–14721

44. Chen I-W, Liang Z, Wang B, Zhang C (2010) Charge-induced asymmetrical displacement of an aligned carbon nanotube buckypaper actuator. Carbon 48(4):1064–1069

45. Hu Y, Chen W, Lu L, Liu J, Chang C (2010) Electromechanical actuation with controllable motion based on a single-walled carbon nanotube and natural biopolymer composite. ACS Nano 4(6):3498–3502

46. Fakhrabadi MMS, Khorasani PK, Rastgoo A, Ahmadian MT (2013) Molecular dynamics simulation of pull-in phenomena in carbon nanotubes with Stone-Wales defects. Solid State Commun 157:38–44

47. Spinks GM, Wallace GG, Fifield LS, Dalton LR, Mazzoldi A, De Rossi D, Khayrullin II, Baughman RH (2002) Pneumatic carbon nanotube actuators. Adv Mater 14(23):1728–1732

48. Rasekh M, Khadem SE (2011) Pull-in analysis of an electrostatically actuated nano-cantilever beam with nonlinearity in curvature and inertia. Int J Mech Sci 53(2):108–115

49. Chen L, Liu C, Liu K, Meng C, Hu C, Wang J, Fan S (2011) High-performance, low-voltage, and easy-operable bending actuator based on aligned carbon nanotube/polymer composites. ACS Nano 5(3):1588–1593

50. Park S, An J, Suk JW, Ruoff RS (2010) Graphene-based actuators. Small 6(2):210–212

51. Kang JW, Hwang HJ (2004) Gigahertz actuator of multiwall carbon nanotube encapsulating metallic ions: molecular dynamics simulations. J Appl Phys 96(7):3900–3905

52. Li J, Ma W, Song L, Niu Z, Cai L, Zeng Q, Zhang X et al (2011) Superfast-response and ultrahigh-power-density electromechanical actuators based on hierarchal carbon nanotube electrodes and chitosan. Nano Lett 11(11):4636–4641

53. Hernandez E, Goze C, Bernier P, Rubio A (1999) Appl Phys A Mater Sci Process A68:287

54. Baughman RH, Cui C, Zakhidov AA, Iqbal Z, Barisci IN, Spinks GM, Wallace GG, Mazzoldi A, DeRossi D, Rinzler AG, 1aschinski O, Roth S, Kertesz M (1999) Carbon nanotube actuators. Science 284:1340

55. Kim P, Lieber CM (1999) Nanotube nanotweezers. Science 286:2148

56. Zhang Y, Iijima S (1999) Elastic response of carbon nanotube bundles to visible light. Phys Rev Lett 82:3472

57. Baughman RH, Cui C, Zakhidov AA, Iqbal Z, Barisci JN, Spinks GM, Wallace GG et al (1999) Carbon nanotube actuators. Science 284(5418):1340–1344

58. Reddy JN (1993) An introduction to the finite element mehtod. McGraw-Hill, New York

59. Zienkiewicz OC, Taylor RL (1991) The Finite element method: nonlinear problems. McGraw-Hill, New York, vol. 20

60. Ouakad HM (2015) Numerical model for the calculation of the electrostatic force in non-parallel electrodes for MEMS applications. J Electrostat 76:254–261

61. Ouakad HM (2014) Static response and natural frequencies of microbeams actuated by out-of-plane electrostatic fringing-fields. Int J Non-Linear Mech 63:39–48

62. Chen X, Wu Z (2017) Review on macromodels of MEMS sensors and actuators. Microsyst Technol 23(10):4319–4332

63. Firaque MT, Ouakad HM (2016) Static, eigenvalue problem and bifurcation analysis of MEMS arches actuated by electrostatic fringing-fields. Microsystem Technol 22(1):193–206

64. Ouakad HM (2016) Electrostatic fringing-fields effects on the structural behavior of MEMS shallow arches. Microsyst Technol 1:1–9

65. Ouakad, Sedighi HM (2016) Rippling effect on the structural response of electrostatically actuated single-walled carbon nanotube based NEMS actuators. Int J Non-Linear Mech 87:97–108

66. Ouakad HM, Younis MI (2013) Modeling the structural-thermal-electrical coupling in an electrostatically actuated MEMS switch and its impact on the switch stability. Math Probl Eng 6:1–8